Annals of Anatomy 255 (2024) 152289

Contents lists available at ScienceDirect

Annals of Anatomy

journal homepage: www.elsevier.com/locate/aanat

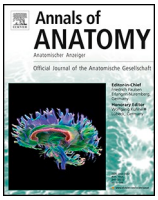

The human dermal white adipose tissue (dWAT) morphology: A multimodal imaging approach

Federico Boschi [a,*,1], Alessandro Negri [b,1], Anita Conti [b], Paolo Bernardi [b], Salvatore Chirumbolo [a], Andrea Sbarbati [b]

[a] Department of Engineering for Innovation Medicine, Strada Le Grazie 8, Verona 37134, Italy
[b] Department of Neurosciences, Biomedicine and Movement Sciences, Strada Le Grazie 8, Verona 37134, Italy

ARTICLE INFO

Keywords:
Dermal white adipose tissue
Adipocyte
Fat
Skin
Magnetic Resonance Imaging
Scanning Electron Microscopy
Optical microscopy

ABSTRACT

Background: Dermal white adipose tissue (dWAT) in humans can be characterized as a relaxed dermal skin compartment consisting of functionally interlinked adipocytes. dWAT is typically discerned both in terms of morphology and function from subcutaneous white adipose tissue (sWAT). In particular in human thigh, the dWAT appears as thin extensions from the adipose panniculus to the dermis, and it is primarily associated with pilosebaceous units, hair follicles, sebaceous glands, and erector pili muscles. In this work, human fat tissue samples obtained post-mortem from the gluteo-femoral region were analyzed focusing on the thin extensions of dWAT named dermal cones. This anatomical region was chosen to deepen the dWAT morphological features of this site which is interesting both for clinical applications and genetical studies. The purpose of this exploratory methodological study was to gain deeper insights into the morphological features of human dWAT through a multimodal imaging approach.

Methods: Optical microscopy, Magnetic Resonance Imaging (MRI) and Scanning Electron Microscopy (SEM), have been employed in this study. The cones' length and their distances were measured on the acquired images for optical microscopy and SEM. The cone's apparent regular distribution in MRI images was evaluated using a mathematical criterion, the conformity *ratio*, which is the *ratio* of the mean nearest-neighbor distance to its standard deviation.

Results: The imaging techniques revealed white adipocytes forming a layer, referred to as sWAT, with cones measuring nearly 2 mm in size measured on SEM and Optical images (2.1 ± 0.4 mm), with the lower part embedded in the sWAT and the upper part extending into the dermis. The distance between the cones results about 1 mm measured on MRI images and they show an overall semiregular distribution.

Conclusions: MRI images demonstrated an orderly arrangement of cones, and their 3D reconstruction allowed to elucidate the dermal cones' disposition in the tissue sample and a more general comprehensive visualization of the entire fat structure within the dermis.

1. Introduction

White adipose tissue (WAT) depots within the human body have become focal points of extensive investigation due to their significant implications across various domains of regenerative medicine and tissue repair processes. Of particular interest within the human integumentary system are two distinct types of adipose tissue: dermal white adipose tissue (dWAT) and subcutaneous white adipose tissue (sWAT). dWAT is characterized as a functional rather than merely anatomical unit as reported in the literature (Kruglikov et al., 2016; Driskell et al., 2014).

dWAT and sWAT differ significantly in terms of gross anatomy and histological characteristics. Previous studies (Smith et al., 2001; Miyazaki et al., 2000; Walker et al., 2007; Sbarbati et al., 2010) have highlighted these distinctions. Notably, dWAT is predominantly associated with pilosebaceous units, hair follicles (HFs), sebaceous glands, and erector pili muscles, while sWAT forms a continuous layer beneath the reticular dermis (Matsumura et al., 2001, Walker et al., 2008, Schmidt et al., 2012, Wojciechowicz et al., 2013).

* Corresponding author.
E-mail address: federico.boschi@univr.it (F. Boschi).
[1] These authors contributed equally to the manuscript

https://doi.org/10.1016/j.aanat.2024.152289
Received 6 October 2023; Received in revised form 2 May 2024; Accepted 27 May 2024
Available online 6 June 2024

dWAT performs various metabolic functions akin to other WAT depots, including lipid storage and release in response to changes in nutrient availability (Sumikawa et al., 2014, Guerrero-Juarez et al., 2018). Considering the substantial surface area of the human body, approximately 2 square meters, dWAT may also play a vital role in thermoregulation and immune functions in humans (Du Bois et al., 1916). Furthermore, dWAT appears to be particularly involved in skin renewal, especially in response to damage, wounds, or stressors (Liu et al., 2012; Segalla et al., 2021).

Current research recognizes that dWAT adipocytes are pivotal in numerous physiological and pathological processes, encompassing temperature regulation (Kasza et al., 2014), protection against skin infections (Zhang et al., 2015), regulation of hair follicles (HF) cycling (Festa et al., 2011), wound healing (Schmidt et al., 2013), skin aging (Rivera-Gonzalez et al., 2014), and cutaneous fibrosis (Marangoni et al., 2015). Specifically, dWAT undergoes remodeling in coordination with the hair cycle, thickening during *anagen* (hair growth) and thinning during *catagen* (regression) to *telogen* (rest) phases (Festa et al., 2011; Guerrero-Juarez et al., 2018). In terms of skin defense following injury, resident adipose progenitors within dWAT become activated near wound edges, migrate into the wound bed, and contribute to fibroblast recruitment, a critical component of scar tissue formation (Schmidt et al., 2013; Shook et al., 2020; Van Hook, 2020).

Human dWAT exhibits a distinctive cone-shaped geometry known as dermal cones, encircling the proximal half of HFs with dermal adipocytes extending from beneath the HF matrix to eccrine sweat glands and the bulge area of HFs (Poblet et al., 2018; Nicu et al., 2018). Dermal cones, first identified in 1950 within the dermis of burning lesions and hypertrophic scars, were hypothesized to play a role in the hypertrophic scarring process. They have a lower portion containing sweat glands, hair follicles and a fat dome, extending into the hypodermal fat, and an upper portion housing the hair shaft, sweat duct, and pilosebaceous unit (Jackson, 1953; Matsumura et al., 2001; Engrav et al., 2011). However, due to scarcity of integrative quantification methods, structures and alignment of these fat cones remained relatively unexplored for many years. As such, the precise role of dWAT in the human body and its interactions with underlying sWAT still remain unclear (Segalla et al., 2021).

To investigate the micro and ultrastructural morphology of healthy dermal white adipose tissue, human samples were collected from the gluteo-femoral region of a cadaver. This anatomical region was chosen to deepen the dWAT morphological features of this site which is interesting both for clinical applications and genetical studies (Agrawal et al., 2022). This study focuses on acquiring and analyzing images of human dWAT obtained through diverse imaging modalities, including optical microscopy, Magnetic Resonance Imaging (MRI), and Scanning Electron Microscopy (SEM). Notably, MRI emerges as a non-invasive technique that can comprehensively elucidate the anatomy of dWAT, especially when augmented with 3D reconstruction capabilities. The MRI images vividly reveal the intricate structure of dWAT, featuring dermal cones extending from sWAT into the dermis, comprised of numerous adipocytes, some of which appear fused together. As such, MRI offers a valuable tool for achieving complete 3D reconstructions of skin fat content, elucidating the distribution of dermal cones with nearly regular spacing within the tissue sample.

2. Material and methods

2.1. Collecting adipose tissue

Four samples of fat tissue from the gluteo-femoral region were collected from a 60-year-old female cadaver by ICLO Teaching and Research Centre in Verona, Italy. These samples were taken from a non-scarred region of healthy skin. After collection, all the samples were fixed in 10 % Neutral Buffered Formalin until usage. Two of these tissue samples were used for this study: one for examining its optical-morphological and ultrastructural structure (first sample) and the other for conducting MRI acquisitions (second sample).

2.2. Staining and stereo microscope imaging

The first sample was cut in half; both sections were washed three times in Phosphate Buffer 0.1 M (PB) for five minutes, stained with 1 % Toluidine Blue for 60 seconds, and then washed again with PB for one minute. Both sections were examined with a Zeiss Stemi SV6 Stereo Microscope (Zeiss, Oberkochen, Germany) (Fig. 1A and Fig. 2A) equipped with a CMOS XS- 26 mm 12 MP, 4032×3024, and the images were acquired with exposure parameters 1/25 s, ISO 500.

2.3. Ultrastructural analysis

The same sections stained with Toluidine Blue, were used for SEM acquisitions. Sections were fixed again in 2 % glutaraldehyde in 0.1 M Phosphate Buffer Solution (PBS), postfixed in 1 % osmium tetroxide in PBS 0.1 M for 1 h, and dehydrated in graded acetones (Fluka, Buchs, Switzerland). The specimens were then treated by a critical point dryer (CPD 030; BAL-TEC AG, Balzers, Liechtenstein), mounted on aluminum stubs with sticky carbon and coated by gold (MED 010; BAL-TEC AG). A XL 30 ESEM (FEI-Philips) scanning electron microscope was used for the ultrastructural examination.

2.4. MRI acquisitions

The second sample was used for MRI. It was washed in PB 0.1 M three times for five minutes, placed in 50 mL tube and filled with PB. Coronal images were collected on a preclinical 7 T small-animal MRI system (Bruker BioSpin, 70/16US; Germany) equipped with a 3.5 cm i.d. transmitter/receiver birdcage coil. Transversal T_2 weighted images were acquired using a 2-dimensional (2D) RARE sequence with the following parameters: TR= 2000 ms, TE = 7 ms, slice number = 60, slice thickness = 150 μm, matrix size = 200 ×200, FOV = 30 ×30 mm, in-plane resolution = 150 ×150 μm^2, number of averages = 250. Images were exported as DICOM using ParaVision software (v.6.0.1; Bruker).

2.5. Creating a 3D model from MR images

To obtain the 3D reconstruction of the dWAT structure, we developed a completely automatic routine using MATLAB R2023a (The MathWorks, Inc., Natick; MA, USA). The routine opens the DICOM files and selects, in each slice, the pixels with MRI signal intensity greater than a threshold determined *a priori* through various attempts on the basis of the image analysis and the expertise of the operator. These pixels are related to dWAT because fat has a higher MR signal.

The set of all selected pixels which, considering the thickness of the slices are voxels, gives the volume of dWAT. Due to the planar resolution of the MRI images (150×150 μm) and the thickness (150 μm), voxels are cubes 150 μm sized. The dWAT volume is smoothed to avoid artifacts using the *smooth3* function of MATLAB, with a filter with a convolution kernel of 5. Finally, the 3D reconstruction was displayed. By moving the position of the virtual camera, a video was recorded (in.avi video format) using the *VideoWriter* MATLAB function showing the three-dimensional dWAT sample from different viewpoints.

2.6. Analyzing the structure in 2D MRI images

To measure the mean distance between cones, a semi-automatic routine was written in MATLAB. The routine is based on tracking a Region of Interest (ROI) containing the dermal cones in the coronal MRI images in DICOM format. Pixels with higher MRI signals than a threshold are isolated from the background and considered related to the cones. The centroid of each cone is identified, and the distances between all the centroids are measured.

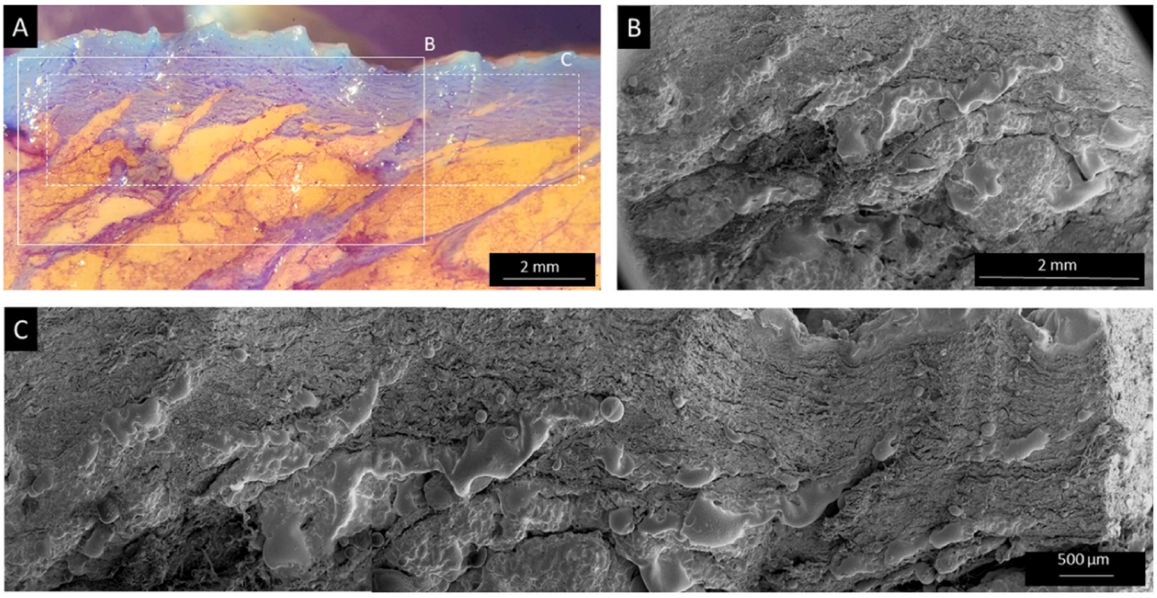

Fig. 1. Stereomicroscope (A) and ultrastructural images (B, C) of dWAT.

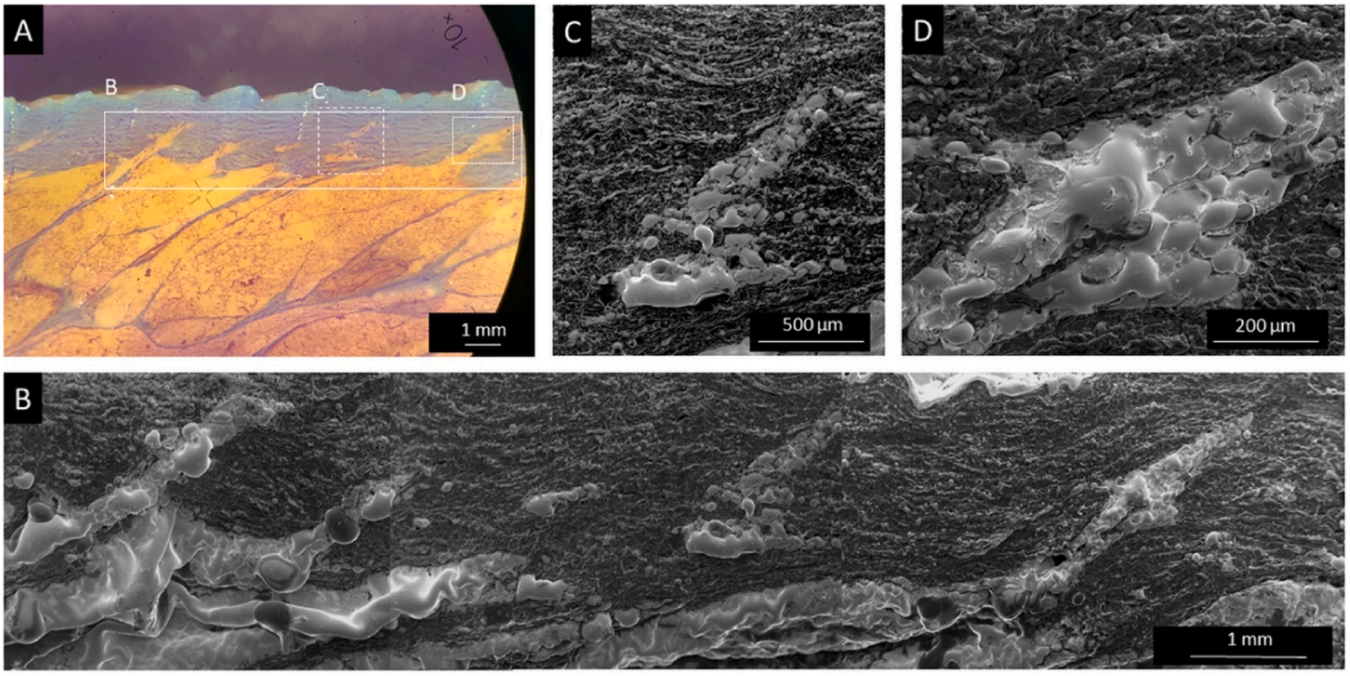

Fig. 2. Another example of stereomicroscope (A) and ultrastructural images (B-D) of dWAT. Magnification of details (C, D).

To describe the regularity of dermal cones' arrangement, three simulation cases were also considered: i) a set of points (centroids) regularly displaced in a rectangular region, ii) a set of points regularly displaced in a circular region, and iii) a set of points randomly displaced in a circular region.

To quantify the regularity of the cones' disposition, a mathematical approach based on the measure of the conformity *ratio* was used. The conformity *ratio* is the *ratio* of the mean nearest-neighbor (MNN) distance to the standard deviation (std) of the nearest-neighbor (NN) distance, i.e.

$$conformity\ ratio = \frac{MNN}{std(NN)}$$

Initially proposed by Wässle and Riemann in 1978, it was applied in literature, for example, to quantify the regular disposition of the mosaics of neurons in the retina (Wässle and Riemann, 1978; Cook, 1996; Allison et al., 2010; Galli-Resta and Novelli, 2000). With the same mean nearest-neighbor distance, the lower its standard deviation, the higher the value of the conformity ratio, which indicates a greater regularity of the pattern (Wässle and Riemann, 1978). The conformity *ratio* was here calculated in the experimental case and in the three simulation cases.

3. Results

3.1. Stereo microscope imaging and ultrastructural analysis

In optical images obtained at the stereo microscope, dWAT appears composed by a layer of adipocytes with dermal cones arising towards the

upper layer of the epidermis. In the observed samples, all the cones sloped at the same angle with respect the basal surface.

These results are confirmed by SEM analysis. Figs. 1 and 2 show two samples observed in both optical and ultrastructural modalities. In the magnification details, the cones appear composed by many adipocytes (Fig. 1 B, C; Fig. 2 B, C, D).

Due to the difficulty of estimating the end of the cone on one side and the surface which constitutes the limit of the compact layer of adipose cells, it is possible to give only an estimate of the length of the cones. Among the best-defined ones, 12 cones were selected, and their length was 2.1 ± 0.4 mm.

3.2. MRI images

The fat content in the dWAT sample is well visible in the coronal MRI images (Fig. 3, with FOV = 30 ×30 mm along x- and y-axis). The lower MRI slices show an adipose layer composed of many large adjacent areas with high MRI signals. Moving upward along the z-axis, the gap between the areas increases, and the areas become smaller and more rounded, forming an almost regular structure of large dots well separated from each other. This structure is the focus of the Sub-Section 3.3.

3.3. 3D reconstruction of MRI images

The 3D reconstruction of the volume of the fat content visible in the MR image reveals a slightly round surface covered by dermal cones almost equally sized and regularly arranged. The cones are almost uniformly sloped with respect the surface. The structures visible in the 3D reconstruction, and in particular the tips of the cones, appear rounded due to the smoothing function used during the 3D reconstruction to reduce artifacts. Fig. 4 shows the dWAT reconstruction. Moving the virtual camera focused on the 3D model it was possible to record a video of the dWAT sample from different angles of view. The video is available in Supplementary Material.

3.4. Structure analysis from 2D MRI images

The focus of this sub-section is the estimation of the distance between dermal cones, i.e., the distance between the centroids defined above on the MRI images. For this purpose, another routine was written in MATLAB, as explained in the Material and Methods Section.

Briefly, it is based on the opening of the images (Fig. 5 A), on the selection of a ROI of interest (Fig. 5B), and on the search for the centroids (Fig. 5 C) of the spots with the greatest signal. The high signal of the spots allows a good identification of the centroids. In the represented image, 47 centroids have been identified.

The centroids are points in a plane (Fig. 6A) of which the coordinates (in pixels) are reported by the MATLAB function *centroids*. Knowing the coordinates, the mutual distance can be measured and converted into millimeters. All the sets of distances can be represented by the distance matrix, in which each pixel is the distance from one point to another one. Of course, all the elements on the diagonal of the matrix, representing the distance between a point and itself, are equal to 0 (Fig. 6B).

The distribution of all distance measurements is shown with histograms in Fig. 6C. The gap between the first bar and the next one indicates a non-zero distance between the nearest centroids. Considering all the measurements (Fig. 6D), the minimum distance between two different points indicates the step of the regular structure, and the average and the standard deviation of the minimum distance can be calculated. The result is: 1.14 mm ±0.42 mm.

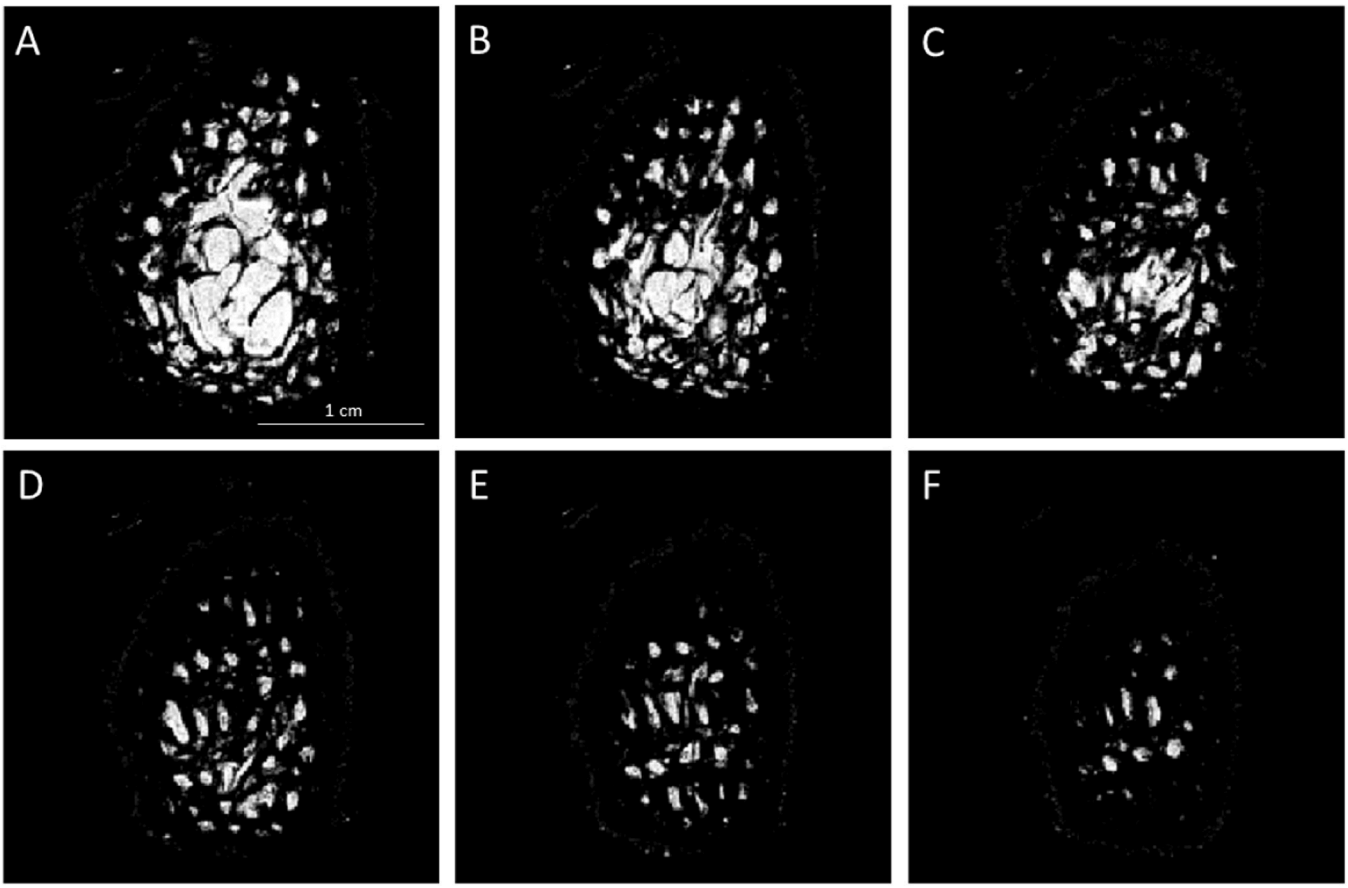

Fig. 3. Coronal MRI images of the dWAT sample obtained with a 7 T tomograph and Turbo RARE sequence. Image parameters: resolution 150 μm, Field of View (FOV, x-axis x y-axis) 30 ×30 mm; the slices (A-F) (150 μm thick) are separated by 300 μm along the z-axis.

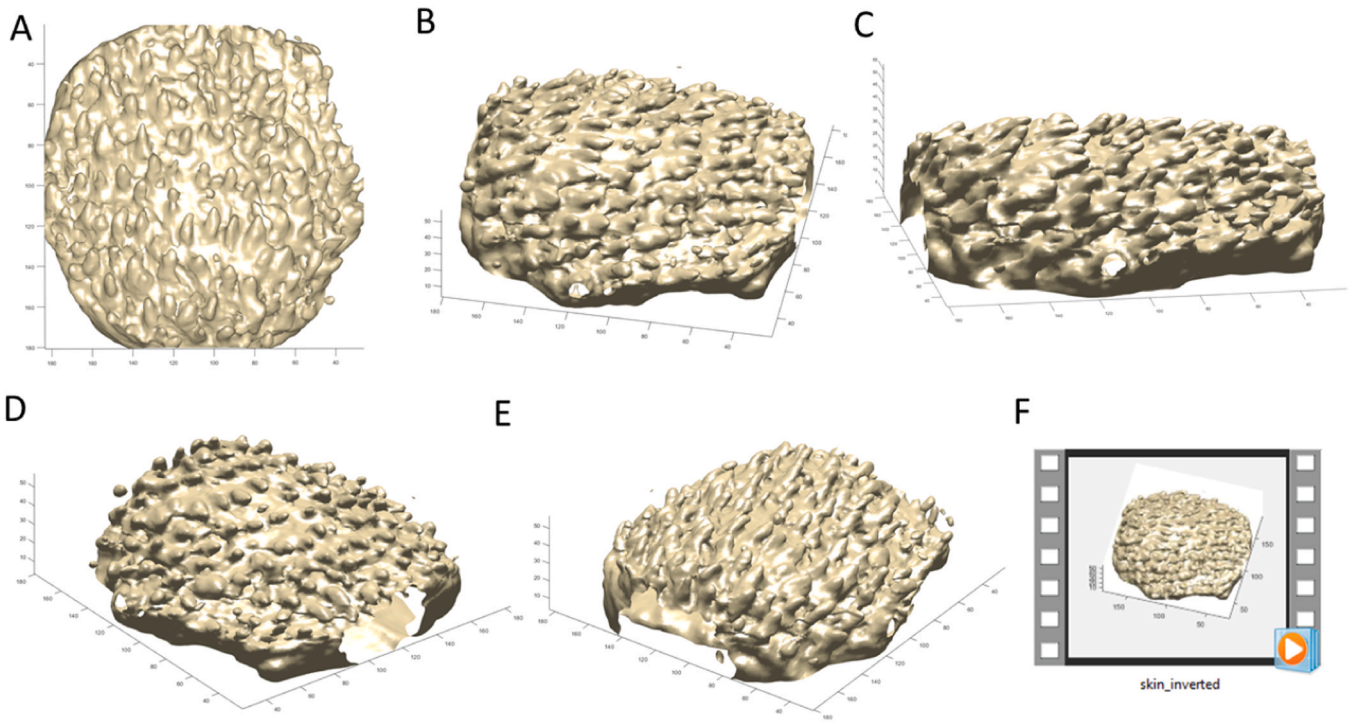

Fig. 4. 3D representation of dWAT sample obtained by MR images at different view angles (A-E). A video recorded moving the camera around the dWAT sample is available in Supplemental Material (F).

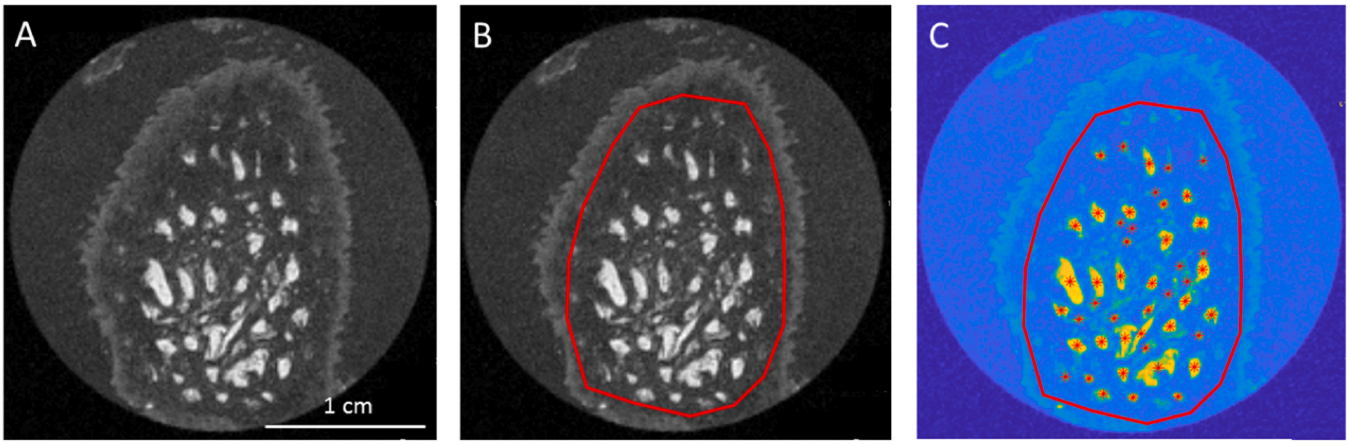

Fig. 5. 2D representation of MRI image used for distance measurement (A). The Region of interest (ROI) manually traced on the MRI image around the dermal cones (B). The centroids (red asterisks) detected by the routine on the MRI images (in false color, C) inside the ROI.

To highlight the almost regular arrangement of the centroids a study was conducted simulating three different points arrangements; two regular and one random. In the first case a number of points (48) similar to the ones of centroids (47) are displaced in rectangular area with 6×8 points (Fig. 6E). The distance between adjacent points is one unit. The distance matrix shows a very regular pattern (Fig. 6F). The distribution plot shows bars well separated (Fig. 6G). Considering for example the first point at the top left of the figure, the distances to points on the same first line are: 1, 2, 3, 4, 5, 6 unit. The distance from the points of the second line are 1, $\sqrt{2}$, $\sqrt{5}$, $\sqrt{10}$…unit. Similar situation occurs taking other points as the starting point. Therefore, certain distance values are particularly frequent. Looking at the overall plot of the measurements (Fig. 6H) it is possible to perceive a regular pattern. Obviously, the mean minimum distance results equal to 1 and the standard deviation is 0 as indicated by the red lines (Fig. 6H).

Since the points corresponding to the vertices of the rectangle are in a special position, another scheme was considered. It is composed by equally spaced points arranged in a circle, within a radius R from a central point (Fig. 6I). To maintain a similar number of points, a radius of 3.9 units was considered. The corresponding circle contains 45 points. Also, in this case the distance matrix shows a clear regularity (Fig. 6J). The considerations regarding the distribution plot and the overall plot of the measurements done for the previous model, still apply here (Figs. 6K and 6L).

In the third case, a set of 47 randomly arranged in a circle 3.9 units radius was taken considered (Fig. 6L). The distance matrix clearly shows that the regularity in distance measurement has been lost (Fig. 6M). The distribution plot of distance shows again a peak at 0 (the distance between each point and itself) but also an almost continuous distribution, indicating that all the measurements between 0 and the maximum value (the distance between the furthest points) are possible (Fig. 6N). The gap between the first bar and the second is also small because some points

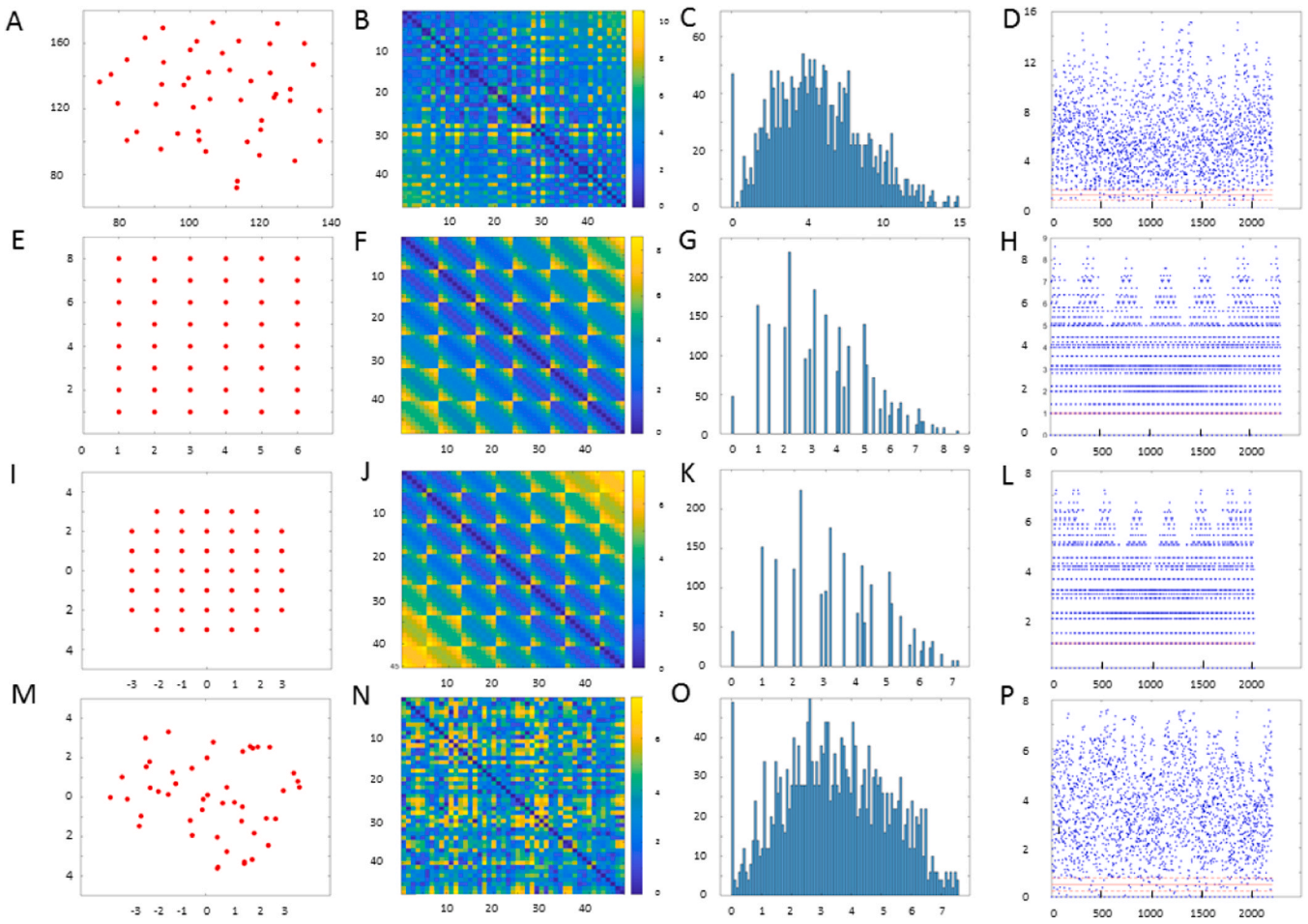

Fig. 6. Centroids distribution (A, E, I, M), matrix of distance (B, F, J, N), histogram of distance distribution (C, G, K, O), distance measurement with the mean minimum distance (as defined in the text) ± std indicated by red line and dotted red lines respectively (D, H, L, P). Real centroids arrangement as obtained by MRI image (first line), regular squared centroids arrangement (second line), regular circular centroids arrangement (third line), random centroids arrangement (fourth line).

can be extremely close.

The mean minimum distance, in this case, is 0.51 ±0.27 units (Fig. 6O).

The comparison between the distance matrices and distance distribution plots shows that the arrangement of centroids found in the MRI images represents an intermediate level between the perfectly regular arrangement of points, as in the first two cases, and the random arrangement. Therefore, it is possible to understand that the arrangement of the dermal cones is quite regular, also taking into account the fact of the experimental errors.

To obtain a mathematical quantification of the regularity, the conformity *ratio* was measured in each simulation case and in the experimental case. In both regular squared and circled disposition, the MNN distance is 1, and the std(NN) is 0, resulting in a conformity *ratio* infinite. In random circled disposition, the MNN distance is 0.47 ± 0.31, resulting in a conformity *ratio* of 1.51. In the experimental case, the MNN distance is 41.68 ± 10.72, resulting in a conformity *ratio* of 3.90.

4. Discussions and conclusions

The primary objective of this investigation is to provide a morphological characterization of dWAT through an exploratory multimodal imaging approach based on optical microscopy, SEM, and MRI. These techniques are assuming an important role in the study of adipose panniculus (Veronese et al., 2021).

A particular emphasis was placed on the dWAT structural components known as dermal cones. Our observations, based on optical, ultrastructural, and MRI imaging, collectively validate the presence of a basal adipocyte layer and a substantial number of dermal cones composed of adipocytes. These dermal cones, approximately 2 mm in length, extend from the basal layer into the dermis. The precise measurement of cone length presents challenges due to the inherent complexities in defining their boundaries and potential variations stemming from sample handling and storage conditions. Moreover, in the observed samples, all the cones exhibited a consistent and similar slope relative to the basal surface, probably due to real inclination or due to fixative and handling procedures.

An estimation of the mean minimum distance between the dermal cones, derived from MRI images, approximates at about 1.14 mm, suggesting a linear density of approximately 10 mm/1.14 mm = 8.77 cones per centimeter. Thus, we can estimate a density of 77 cones per square centimeter. It is noteworthy that the density of HFs in adult thigh or back areas is roughly estimated to be in the range of 30–90 hair follicles per square centimeter (Blume et al., 1991, Otberg et al., 2004). Consequently, we can infer that the MRI technique enables the visualization of nearly all dWAT cones in such area.

Comparative analysis of cones' distance matrices and distance distributions reveals that the arrangement of the cones observed in MRI images falls between a perfectly regular arrangement and a purely random arrangement.

From a mathematical point of view, the value of the conformity *ratio* in the experimental case results in between the values obtained in the

cases of perfect regular disposition and the case of a random disposition, meaning a semi-regular disposition of the cones. This finding lends support to a reconstructed imaging representation portraying dermal cones as moderately regular in their distribution, as obtained from 3D reconstruction modelling, leveraging computational techniques for MRI image reconstruction and analysis.

In our knowledge, the present study represents the first attempt to 3D reconstruct the dWAT in human gluteo-femoral region and to quantify the cone's size and distribution using different imaging techniques.

Moreover, it represents a pioneering utilization of MRI, augmented by MATLAB-based in silico reconstruction, to discern, analyze, and visualize a previously indistinct anatomical compartment like dWAT. This effort aimed to be a preliminary morphological analytical step to address future more extensive research aiming to a comprehensive understanding of dWAT's physiology and biology.

In-depth scrutiny of the dermal cone's structure holds the potential to elucidate their role within dermal fat. The function of human dermal fat, situated beneath the dermis (the outermost skin layer), encompasses cushioning, protection of internal structures, insulation, and energy storage. Noteworthy, the distinctive papilla-like appearance of dWAT, referred to as "adipose papillae," whose function remains elusive, may serve as sensory structures capable of modulating cell dynamics and differentiation/dedifferentiation by probing reactive oxygen species (ROS) signaling (Segalla et al., 2021).

In this study, a single subject only was analyzed, and this fact limits the generalization of the findings. Moreover, it might be interesting to obtain samples from both male and female gender, looking at the features of the dermal cones. Nevertheless, this study has to be considered an exploratory methodological work that could be applied to new investigations on a wider scale.

A comprehensive analysis of dWAT using both traditional morphological techniques together with innovative imaging analytical approach holds the promise of unveiling new insights into this particularly interesting kind of adipose tissue compartment. This approach could address future studies for example in the field of tissue remodeling and wound repair.

CRediT authorship contribution statement

Andrea Sbarbati: Writing – original draft, Supervision, Resources, Methodology, Investigation, Conceptualization. **Federico Boschi:** Writing – review & editing, Writing – original draft, Software, Methodology, Investigation. **Salvatore Chirumbolo:** Writing – review & editing, Writing – original draft. **Paolo Bernardi:** Methodology, Investigation. **Anita Conti:** Writing – review & editing, Methodology, Investigation. **Alessandro Negri:** Writing – review & editing, Writing – original draft, Methodology, Investigation.

Declaration of Competing Interest

The authors declare that they have no known competing financial interests or personal relationships that could have appeared to influence the work reported in this paper.

Acknowledgements

The authors would like to thank the Technological Platform Center (CPT) of the University of Verona for the Magnetic Resonance Tomograph usage.

Ethical_statement

Not applicable

Artificial Intelligence

During the preparation of this work the authors used ChatGPT in order to improve readability and language. After using this tool, the authors reviewed and edited the content as needed and take full responsibility for the content of the publication.

Appendix A. Supporting information

Supplementary data associated with this article can be found in the online version at doi:10.1016/j.aanat.2024.152289.

References

Agrawal, S., Wang, M., Klarqvist, M.D.R., Smith, K., Shin, J., Dashti, H., Diamant, N., Choi, S.H., Jurgens, S.J., Ellinor, P.T., Philippakis, A., Claussnitzer, M., Ng, K., Udler, M.S., Batra, P., Khera, A.V., 2022. Inherited basis of visceral, abdominal subcutaneous and gluteofemoral fat depots. Nat. Comm. 13, 3771.

Allison, W.T., Barthel, L.K., Skebo, K.M., Takechi, M., Kawamura, S., Raymond, P.A., 2010. Ontogeny of cone photoreceptor mosaics in zebrafish. J. Comp. Neurol. 518 (20), 4182–4195.

Blume, U., Ferracin, J., Verschoore, M., Czernielewski, J.M., Schaefer, H., 1991. Physiology of the vellus hair follicle: hair growth and sebum excretion. Br. J. Dermatol. 124, 21–28.

Cook, J.E., 1996. Spatial properties of retinal mosaics: an empirical evaluation of some existing measures. Vis. Neurosci. 13 (1), 15–30.

Driskell, R.R., Jahoda, C.A., Chuong, C.M., Watt, F.M., Horsley, V., 2014. Defining dermal adipose tissue. Exp. Dermatol. 23 (9), 629–631.

Du Bois, D., Du Bois, E.F., 1916. A formula to estimate the approximate surface area if height and weight be known. Arch. Intern. Med. 17 (6), 863–871.

Engrav, L.H., Tuggle, C.K., Kerr, K.F., et al., 2011. Functional genomics unique to week 20 post wounding in the deep cone/fat dome of the duroc/yorkshire porcine model of fibroproliferative scarring. PLoS ONE 6 (4), e19024.

Festa, E., Fretz, J., Berry, R., Schmidt, B., Rodeheffer, M., Horowitz, M., Horsley, V., 2011. Adipocyte lineage cells contribute to the skin stem cell niche to drive hair cycling. Cell 146, 761–771.

Galli-Resta, L., Novelli, E., 2000. The effects of natural cell loss on the regularity of the retinal cholinergic arrays. J. Neurosci.: Off. J. Soc. Neurosci. 20 (3), RC60.

Guerrero-Juarez, C.F., Plikus, M.V., 2018. Emerging nonmetabolic functions of skin fat. Nat. Rev. Endocrinol. 14 (3), 163–173.

Jackson, D.M., 1953. The diagnosis of the depth of burning. Brit J. Surg. 40, 588–596.

Kasza, I., Suh, Y., Wollny, D., Clark, R.J., Roopra, A., Colman, R.J., MacDougald, O.A., Shedd, T.A., Nelson, D.W., Yen, M.I., Yen, C.L., Alexander, C.M., 2014. Syndecan-1 is required to maintain intradermal fat and prevent cold stress. PLoS Genet 10, e1004514.

Kruglikov, I.L., Scherer, P.E., 2016. Dermal adipocytes: from irrelevance to metabolic targets? Trends Endocrinol. Metab. 27 (1), 1–10.

Liu, G.S., Chan, E.C., Higuchi, M., Dusting, G.J., Jiang, F., 2012. Redox mechanisms in regulation of adipocyte differentiation: beyond a general stress response. Cells 1 (4), 976–993.

Marangoni, R.G., Korman, B.D., Wei, J., Wood, T.A., Graham, L.V., Whitfield, M.L., Scherer, P.E., Tourtellotte, W.G., Varga, J., 2015. Myofibroblasts in murine cutaneous fibrosis originate from adiponectin-positive intradermal progenitors. Arthritis Rheuma 67, 1062–1073.

Matsumura, H., Engrav, L.H., Gibran, N.S., Yang, T.M., Grant, J.H., Yunusov, M.Y., Fang, P., Reichenbach, D.D., Heimbach, D.M., Isik, F.F., 2001. Cones of skin occur where hypertrophic scar occurs. Wound Repair Regen. 9, 269–277.

Miyazaki, M., Kim, Y.C., Gray-Keller, M.P., Attie, A.D., Ntambi, J.M., 2000. The biosynthesis of hepatic cholesterol esters and triglycerides is impaired in mice with a disruption of the gene for stearoyl-CoA desaturase 1. J. Biol. Chem. 275 (39), 30132–30138.

Nicu, C., Pople, J., Bonsell, L., Bhogal, R., Ansell, D.M., Paus, R., 2018. A guide to studying human dermal adipocytes in situ. Exp. Dermatol. 27 (6), 589–602.

Otberg, N., Richter, H., Schaefer, H., Blume-Peytavi, U., Sterry, W., Lademann, J., 2004. Variations of hair follicle size and distribution in different body sites. J. Invest Dermatol. 122 (1), 14–19.

Poblet, E., Jimenez-Acosta, F., Escario-Travesedo, E., Hardman, J.A., Hernández-Hernández, I., Agudo-Mena, J.L., Cabrera-Galvan, J.J., Nicu, C., Paus, R., 2018. Eccrine sweat glands associate with the human hair follicle within a defined compartment of dermal white adipose tissue. Br. J. Dermatol. 178 (5), 1163–1172.

Rivera-Gonzalez, G., Shook, B., Horsley, V., 2014. Adipocytes in skin health and disease. Cold Spring Harb. Perspect. Med 4 (3), a015271.

Sbarbati, A., Accorsi, D., Benati, D., Marchetti, L., Orsini, G., Rigotti, G., Panettiere, P., 2010. Subcutaneous adipose tissue classification. Eur. J. Histochem, 25 54 (4), e48.

Schmidt, B., Horsley, V., 2012. Unravelling hair follicle-adipocyte communication. Exp. Dermatol. 21, 827–830.

Schmidt, B.A., Horsley, V., 2013. Intradermal adipocytes mediate fibroblast recruitment during skin wound healing. Development 140, 1517–1527.

Segalla, L., Chirumbolo, S., Sbarbati, A., 2021. Dermal white adipose tissue: much more than a metabolic, lipid-storage organ? Tissue Cell 71, 101583.

Shook, B.A., Wasko, R.R., Mano, O., Rutenberg-Schoenberg, M., Rudolph, M.C., Zirak, B., Rivera-Gonzalez, G.C., López-Giráldez, F., Zarini, S., Rezza, A., Clark, D.A.,

Rendl, M., Rosenblum, M.D., Gerstein, M.B., Horsley, V., 2020. Dermal adipocyte lipolysis and myofibroblast conversion are required for efficient skin repair. Cell Stem Cell 26 (6), 880–895.e6.
Smith, S.R., Lovejoy, J.C., Greenway, F., Ryan, D., deJonge, L., de la Bretonne, J., Volafova, J., Bray, G.A., 2001. Contributions of total body fat, abdominal subcutaneous adipose tissue compartments, and visceral adipose tissue to the metabolic complications of obesity. Metabolism 50 (4), 425–435.
Sumikawa, Y., Inui, S., Nakajima, T., Itami, S., 2014. Hair cycle control by leptin as a new anagen inducer. Exp. Dermatol. 23, 27–32.
Van Hook, A.M., 2020. Fat cells helps wound heal. Sci. Signal. 10 (639), eabd6235.
Veronese, S., Picelli, A., Smania, N., Sbarbati, A., 2021. Hypodermis involvement in skin disorders: imaging and functional imaging diagnostic tools. Ski. Res Technol. 27 (4), 641–643.
Walker, G.E., Marzullo, P., Verti, B., Guzzaloni, G., Maestrini, S., Zurleni, F., Liuzzi, A., Di Blasio, A.M., 2008. Subcutaneous abdominal adipose tissue subcompartments: potential role in rosiglitazone effects. Obesity 16, 1983–1991.
Walker, G.E., Verti, B., Marzullo, P., Savia, G., Mencarelli, M., Zurleni, F., Liuzzi, A., Di Blasio, A.M., 2007. Deep subcutaneous adipose tissue: a distinct abdominal adipose depot. Obesity 15 (8), 1933–1943.
Wässle, H., Riemann, H.J., 1978. The mosaic of nerve cells in the mammalian retina. Proc. R. Soc. B 200, 441–461.
Wojciechowicz, K., Gledhill, K., Ambler, C.A., Manning, C.B., Jahoda, C.A., 2013. Development of the mouse dermal adipose layer occurs independently of subcutaneous adipose tissue and is marked by restricted early expression of FABP4. PLoS One 8 (3), e59811.
Zhang, L.J., Guerrero-Juarez, C.F., Hata, T., Bapat, S.P., Ramos, R., Plikus, M.V., Gallo, R. L., 2015. Innate immunity. Dermal adipocytes protect against invasive Staphylococcus aureus skin infection. Science 347, 67–71.